



**AALBORG UNIVERSITY**  
DENMARK

**Aalborg Universitet**

## **Recognition of Power Quality Issues Associated With Grid Integrated Solar Photovoltaic Plant in Experimental Framework**

Mahela, Om Prakash; Shaik, Abdul Gafoor; Gupta, Neeraj; Khosravy, Mahdi; Khan, Baseem; Alhelou, Hassan Haes; Padmanaban, Sanjeevikumar

*Published in:*  
I E E Systems Journal

*DOI (link to publication from Publisher):*  
[10.1109/JSYST.2020.3027203](https://doi.org/10.1109/JSYST.2020.3027203)

*Publication date:*  
2021

*Document Version*  
Accepted author manuscript, peer reviewed version

[Link to publication from Aalborg University](#)

*Citation for published version (APA):*  
Mahela, O. P., Shaik, A. G., Gupta, N., Khosravy, M., Khan, B., Alhelou, H. H., & Padmanaban, S. (2021). Recognition of Power Quality Issues Associated With Grid Integrated Solar Photovoltaic Plant in Experimental Framework. *I E E Systems Journal*, 15(3), 3740-3748. [9228883].  
<https://doi.org/10.1109/JSYST.2020.3027203>

### **General rights**






Copyright and moral rights for the publications made accessible in the public portal are retained by the authors and/or other copyright owners and it is a condition of accessing publications that users recognise and abide by the legal requirements associated with these rights.

- Users may download and print one copy of any publication from the public portal for the purpose of private study or research.
- You may not further distribute the material or use it for any profit-making activity or commercial gain
- You may freely distribute the URL identifying the publication in the public portal -

### **Take down policy**

If you believe that this document breaches copyright please contact us at [vbn@aub.aau.dk](mailto:vbn@aub.aau.dk) providing details, and we will remove access to the work immediately and investigate your claim.

# Recognition of Power Quality Issues Associated With Grid Integrated Solar Photovoltaic Plant in Experimental Framework

Om Prakash Mahela , Senior Member, IEEE, Abdul Gafoor Shaik , Neeraj Gupta, Mahdi Khosravy, Baseem Khan , Member, IEEE, Hassan Haes Alhelou , and Sanjeevikumar Padmanaban , Senior Member, IEEE

**Abstract**—Enhancement in solar energy (SE) injection into the power system network creates power quality (PQ) issues in the supply. This article presents an approach supported by Stockwell transform ( $S$ -transform) for assessment of PQ issues related with the grid interfaced solar photovoltaic (SPV) system under various operating conditions. This will help to enhance the SE integration level into the utility grid. The set up, to perform assessment of the PQ issues includes an emulated SPV system interfaced with the utility at the point of common coupling (PCC). Measurements of voltage and current signals are performed by utilizing power network analyzer. The captured voltage signals are analyzed using  $S$ -transform for the detection of a variety of PQ problems associated with the grid interfacing and outage of the SPV system. Effects on PQ due to presence of the various types of loads at PCC have also been investigated under the same operating conditions. Effect of partial shading of SPV plates on the PQ is also investigated. Harmonic analysis is performed for all the investigated events. The proposed algorithm proved to be successful for detecting different PQ disturbances under all the investigated operating conditions.

**Index Terms**—Power quality (PQ), solar energy (SE), solar photovoltaic (SPV) system, Stockwell transform ( $S$ -transform), utility grid.

## I. INTRODUCTION

**S**OURCES of renewable energy (RE) generation have come out as a vital solution to issues such as pollution, global

Manuscript received March 5, 2020; revised May 13, 2020 and August 18, 2020; accepted September 21, 2020. (Corresponding author: Om Prakash Mahela.)

Om Prakash Mahela is with the Power System Planning Division, Rajasthan Rajya Vidyut Prasaran Nigam, Ltd., Jaipur 302005, India (e-mail: opmahela@gmail.com).

Abdul Gafoor Shaik is with the Indian Institute of Technology Jodhpur, Jodhpur 342037, India (e-mail: saadgafoor@iitj.ac.in).

Neeraj Gupta is with the Department of Computer Science and Engineering, Oakland University, Rochester, MI 48309 USA (e-mail: neerajgupta@oakland.edu).

Mahdi Khosravy is with the Media Integrated Communication Laboratory, Graduate School of Engineering, Osaka University, Osaka 565-0871, Japan (e-mail: mahdi.khosravy@nanase.comm.eng.osaka-u.ac.jp).

Baseem Khan is with the Department of Electrical Engineering, Hawassa University, Awassa 05, Ethiopia (e-mail: baseem.khan04@gmail.com).

Hassan Haes Alhelou is with the Department of Electrical and Computer Engineering, Isfahan University of Technology, Isfahan 84156-83111, Iran, and also with the Department of Electrical Power Engineering, Tishreen University, Lattakia 2230, Syria (e-mail: alhelou@tishreen.edu.sy).

Sanjeevikumar Padmanaban is with the Department of Energy Technology, Aalborg University, Esbjerg 2230, Denmark (e-mail: san@et.aau.dk).

Digital Object Identifier 10.1109/JSYST.2020.3027203

warming, and rising energy demand [1]. Therefore, academicians, researchers, government sectors, and utilities altogether are trying to integrate RE sources into the utility grids. Recently, the wind and solar energies are promoted worldwide as distributed generation (DG) sources at distribution level for the generation of electricity. The solar photovoltaic (SPV) system based energy is being developed very fast in the global scenario due to its low operating cost and zero pollution. However, the unpredictable nature of solar radiations leads to the unreliable performance of the SPV system associated with the utility [2]. The operational events of SPV systems affect power quality (PQ) of distribution networks to a large extent. Thus, significant voltage transients are likely to occur during synchronization and outage of the SPV system due to large current variations [3].

PQ issues, which include harmonics, voltage fluctuations, reactive power compensation, reverse power flow and power factor, limit the integration level of SPV generation into the grid [4]. Higher penetration levels may cause operating problems such as rejection of solar PV generators due to the presence of PQ disturbances. Such refusal can avoid the penetration of SPV generators to the grid [5]. Thus, assessment of PQ has vital importance in deciding the permissible levels of SPV energy in the utility grid. This PQ assessment has the importance, especially in case of weak utility grid, where the current transients are likely to cause large magnitude of voltage fluctuations.

Various PQ studies reported in the works of the literature have considered different aspects such as type of solar PV plates, converter, design, and insolation variations. Rodriguez *et al.* [6] investigated the voltage unbalance sensitivity for the different penetration levels in Spain distribution feeder, which helps us to define the optimal penetration level. Urbanetz *et al.* [5] presented the evaluation of PQ in the grid feeder of Brazil with a solar PV system. Investigations of PQ issues in the grid with RE sources due to changes in load and environmental characteristic is reported in [7] and [8]. The PQ issues related to design constraints of PV inverters were detailed in [4]. The Stockwell transform ( $S$ -transform) and fuzzy  $C$ -means clustering-based method to recognize the PQ events associated with solar energy penetration using a simulation approach was reported in [9]. Silva *et al.* [10] investigated the effects of SPV interconnection by the utilization of PQ indexes (PQI). PQ issues like long term voltage variations and voltage unbalance were reported in the same research. A transient model of PV plant, which is

utilized for the PQ studies was presented in [11]. Plangklang *et al.* [12] illustrated a simulation work for detecting the PQ issues such as voltage swell, sag, frequency variations, total harmonic distortions (THDs) and voltage ripple associated with the rooftop PV, interfaced to the Thailand grid. Mahela *et al.* [13] investigated the PQ issues associated with the operating scenarios of SPV such as synchronization, outage, and solar insolation deviations using discrete wavelet transform. In [14], authors investigated the possible negative impacts of continuous operation of SPV on the PQ parameters of the power utility network. The impacts of current and voltage harmonics on performances of the grid integrated SPV and their mitigation using the active power filter is reported in [15]. A detailed study of the issues related to voltage quality due to grid interfacing of SPV and their working characteristics are analyzed and presented in [16]. In [17], authors introduced an  $S$ -transform supported method to recognize the PQ issues linked to operating events in the grid by the penetration of wind energy (WE). A variety of operational issues are rated in terms of PQ using the proposed PQI. In [18], a technique for recognition of the inter harmonics, because of design constraints of controller is utilized to integrate SPV with the grid. In [19], authors introduced a detailed study for assessment of the PQ and identification of operational issues in the WE integrated distribution system with the help of  $S$ -transform and fuzzy clustering.

Various techniques utilized to process the signals, such as Hilbert–Huang transform,  $S$ -transform, Fourier transform (FT), wavelet transform (WT), and short-time Fourier transform (STFT), which are widely used to detect various PQ disturbances. Due to the fixed window size, the performance of the STFT is limited. Although, WT with changeable size of window is established to be useful for detecting and locating different contents of frequency by overcoming the restrictions of STFT. But the performance of the WT is considerably influenced due to the availability of noise in the electrical signal [20].  $S$ -transform can minimize the disadvantages associated with the WT due to its capability of performing rationally accurate magnitude and phase spectrum of the investigated signals when noise is present [20], [21]. Artificial intelligent methods such as fuzzy  $C$ -means clustering, genetic algorithm, neural network, fuzzy expert system, and support vector machine are used to classify different PQ problems [20].

This article presents an experimental study of PQ problems linked to the various operating scenarios of SPV plant connected to the grid. The experimental set up includes a single-phase SPV integrated with an emulated grid through the point of common coupling (PCC) with various types of loads. Operational events considered for the investigation include synchronization and outage. These operational scenarios are different from the cases encountered in any SPV system such as outage during night time and passing of clouds. The effects of variation in solar insolation (passing of clouds) are environmental effects of the solar PV system on the PQ, which have already been reported in the literature. Proposed article investigates the effects of sudden interfacing of the SPV plant to the utility grid and its sudden outage from the utility grid, on the quality of power. PQ evaluation is performed for operating scenarios of interfacing

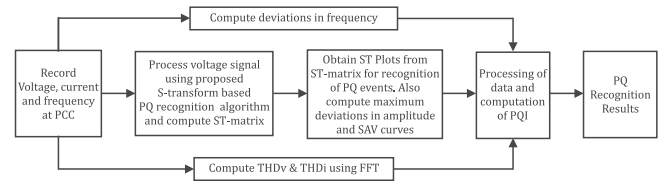


Fig. 1. Block scheme of PQ assessment.

and outage of SPV in the availability of a variety of demands at the same point. Voltage and current signals are recorded at PCC at the time of different operating scenarios of this study. The captured voltage waveforms are analyzed by utilizing multiresolution based on  $S$ -transform for investigating various PQ events. The published literature mainly focused on the PQ issues because of solar insolation variation, converters, and SPV plates design constraints but missed the operational scenarios, which are introduced in this article. Main contributions of this article is detailed as follows.

- 1) This article proposed an approach using  $S$ -transform based plots for recognition of PQ disturbances related to the various operating scenarios such as interfacing and outage of the SPV system, integrated with the grid in experimental framework. This is achieved using the plots such as sum absolute values (SAV), frequency contour (FC), frequency-amplitude (FM) plot, and amplitude plot.
- 2) Furthermore, as specific contribution, this article proposed the SAV plot for enhancing the performance of  $S$ -transform to analyze the PQ events.
- 3) Introduction of PQ assessment at the time of operational scenarios of interfacing and outage, the proposition of PQI for identifying the PQ problems linked to the utility interfacing an SPV are the major contributions of this article.
- 4) Analysis of the harmonics associated with the investigated operational events is also performed to find the level of different harmonics during the events.
- 5) This article will help to find out the PQ issues linked to the utility interfaced SPV. This will help to initiate suitable PQ mitigation method to minimize these disturbances. Furthermore, this will help for enhancing the SE integration level in the grid.

This article is structured into six segments. Section II presents the improved  $S$ -transform based methodology for PQ assessment, proposed PQI and mathematical formulation for proposed algorithm. Section III presents the experimental hardware and data acquisition system (DAS). The experimental results and their analysis using the proposed algorithm are presented in Section IV. Section V deals with the comparison of various case studies, followed by conclusion in the Section VI.

## II. $S$ -TRANSFORM-BASED PQ RECOGNITION ALGORITHM

Fig. 1 describes the proposed algorithm used to recognize the PQ disturbances. Input signal to this algorithm is voltage and current recorded from the hardware set-up and processed using the proposed algorithm in the MATLAB software. It has three major

processing stages for PQ recognition. First stage includes the computation of maximum deviation in the recorded frequency by directly monitoring the frequency. The second stage performs the processing of voltage signals recorded from hardware set-up in MATLAB software using the  $S$ -transform based algorithm at a sampling frequency of 1 kHz to obtain different feature plots. The third stage performs the computation of THDs in recorded voltage and current by utilizing the fast Fourier transform (FFT). PQ problems are linked to the variety of operational scenarios of the PV system while feeding power to the different types of demands, which are processed by utilizing  $S$ -transform supported multiresolution of voltage waveforms with the help of MATLAB software. Three feature plots, i.e., time-FC (namely frequency or  $S$ -contour), amplitude-time (AM) curve, and FM curve are computed through the  $S$ -transform depended multiresolution investigation of the voltage signals. For normalization of the parameters, maximum values are utilized. To improve the performance of the developed technique, a plot designated as SAV plot is specifically introduced in this article. Sum of absolute values of each column of the  $S$ -matrix is utilized to obtain the SAV curve. For detecting the PQ issues related to various operating scenarios, these feature curves are utilized. Deviations in the proposed amplitude curve and SAV curve will help to recognize the magnitude related PQ issues such as sag, swell, and momentary interruption (MI). The FM curve and FC will help us to recognize the frequency-related disturbances such as harmonics and frequency variations. However, all types of curves and contour will help us to recognize the PQ disturbances, i.e., impulsive transient (IT), oscillatory transient (OT), flicker, etc. Hence, by analysis of the proposed  $S$ -transform based plots, all types of PQ disturbances can be recognized effectively. Furthermore, FFT is employed to compute the total harmonic distortions in voltage ( $\text{THD}_v$ ) and current ( $\text{THD}_i$ ) signals. By constant monitoring of the system frequency, deviations in the power frequency are detected in this article. As mentioned above discussed features would be used to recognize the individual PQ issues, i.e., voltage sag, swell, fluctuations, MI, IT, OT, spike, harmonics, flicker, frequency variations, etc. However, the simultaneous incidence of one or more of these PQ disturbances may reduce the effect of one another or sometimes may also increase the effect. Hence, to investigate the effect of simultaneous incidence of these PQ disturbances due to solar PV operations and partial shading conditions in the presence of different nature of loads, the above-mentioned features are utilized to compute a PQI, which is used to rate the different operating scenarios concerning the PQ as detailed in (1). Furthermore, the proposed approach will recognize the PQ disturbances due to the load dynamics. The algorithm is successfully validated to recognize the standard PQ disturbances reported in [22] and [23]. In these signals, the dynamics of the disturbances is relatively higher compared to the signals of the real-time power system network with solar energy penetration.

Computational complexity of the algorithm will depend on the number of samples. At a sampling frequency of 1 kHz (20 samples per cycle), the maximum computational time is 0.051 s whereas at a sampling frequency of 2 kHz (40 samples per cycle), the maximum computational time is 0.162 s. Hence,

when sampling frequency is increased twice then computational time will increase by 3.176 times. Furthermore, size of the  $S$ -matrix also increases with increase in the sampling frequency, which requires large storage capacity. If sampling frequency is decreased below 1 kHz, then some information may be lost. Therefore, optimum sampling frequency for the proposed study is considered equal to 1 kHz. The proposed algorithm will be implemented in the online PQ monitoring devices where actual waveforms will be taken from the real-time network of power and these will be processed in the software using the proposed algorithm and display the identified PQ events.

#### A. Power Quality Index

Maximum deviations in the magnitude and SAV curve, power frequency,  $\text{THD}_v$ , and  $\text{THD}_i$  are utilized to define the PQI, which rate the operating scenarios of the PV system in terms of PQ. Time instants of PQ problems are also taken into considerations to calculate PQI. The following equation computes the PQI:

$$\text{PQI} = \left( \frac{|\Delta A|t_1 + |\Delta S|t_2 + |\Delta f|t_3 + \text{THD}_v + \text{THD}_i}{5} \right) \times 100 \quad (1)$$

where  $\Delta A$  (unit less),  $\Delta S$  (unit less), and  $\Delta f$  (unit is hertz but only magnitude is considered) illustrated the maximum deviations in the AM curve, SAV curve, and in power frequency, correspondingly.  $\text{THD}_v$  and  $\text{THD}_i$  correspond to the  $\text{THD}_v$  and current, correspondingly.  $t_1$ ,  $t_2$ , and  $t_3$  characterize the time duration of the disturbances in AM, SAV, and frequency. For the higher amount of PQI, quality of power in the grid is greatly impacted. Hence, this PQI is utilized in the PQ monitoring components to observe the combined effect of all PQ disturbances on the quality of power.

#### B. Stockwell Transform

Spectrum phase and magnitude contain the information about the PQ disturbance. For utilizing the information presented in phase of the continuous WT (CWT), modification is made in the phase of mother wavelet. This section details with the process of decomposition of a signal  $h(t)$  using the  $S$ -transform. Hence, units will depend on the nature of function  $h(t)$ . The voltage signal is considered as  $h(t)$ , which has the unit volt (V). The CWT of the function  $h(t)$  is described as [24]

$$W(\tau, a) = \int_{-\infty}^{\infty} h(t)\omega(t - \tau, a)dt \quad (2)$$

where  $\omega(t, d)$  represents the scaled replica of fundamental mother wavelet, and  $d$  represents dilation. Dilation factor is the inverse of the frequency [25].

By multiplying the CWT with a phase factor,  $S$ -transform of the function  $h(t)$  is obtained [26]

$$S(\tau, f) = e^{i2\pi ft}W(\tau, d). \quad (3)$$

Furthermore, the mother wavelet is described as follows [24]:

$$w(t, f) = \frac{|f|}{\sqrt{2\pi}} e^{-\frac{t^2 f^2}{2}} e^{-i2\pi ft}. \quad (4)$$

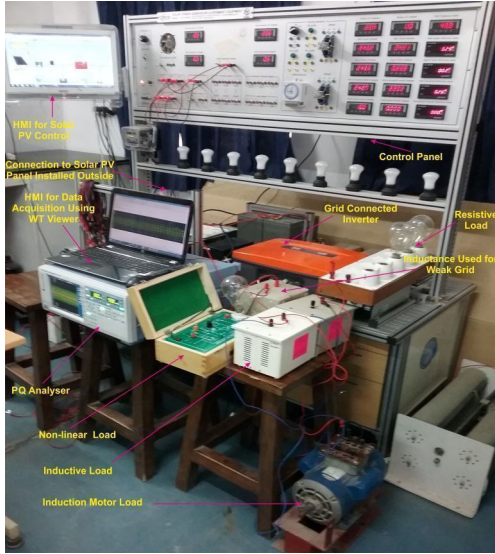


Fig. 2. Experimental set-up of the PQ measurement system.

Hence,  $S$ -transform in the explicit form is presented as follows [24]:

$$S(\tau, f) = \int_{-\infty}^{\infty} h(t) \frac{|f|}{\sqrt{2\pi}} e^{-\frac{(\tau-t)^2 f^2}{2}} e^{-i2\pi f t} dt. \quad (5)$$

Signal  $h(t)$  that represents the PQ disturbance is defined in discrete-time series as  $h[kT]$ ,  $k = 0, 1, \dots, N-1$  with sampling time  $T$ . For time series  $h(t)$ , the discrete FT is presented as [27]

$$H \left[ \frac{n}{NT} \right] = \frac{1}{N} \sum_{k=0}^{N-1} h[kT] e^{-\frac{i2\pi n k}{N}} \quad (6)$$

where  $n = 0, 1, \dots, N-1$ . Explicit representation of the  $S$ -transform of the  $h[kT]$  is described as (letting  $f \rightarrow n/NT$  and  $\tau \rightarrow jT$ ) [26]

$$S \left[ jT, \frac{n}{NT} \right] = \sum_{m=0}^{N-1} H \left[ \frac{m+n}{NT} \right] e^{-\frac{2\pi^2 m^2}{n^2}} e^{\frac{i2\pi m j}{N}}; n \neq 0 \quad (7)$$

and for  $n = 0$  voice, it is described as

$$S [jT, 0] = \frac{1}{N} \sum_{m=0}^{N-1} H \left[ \frac{m}{NT} \right]. \quad (8)$$

The outcome of  $S$ -transform is computed as the complex  $N \times M$  matrix represented as the  $S$ -matrix. The column of this matrix corresponds to definite time while the row of this matrix is related to the definite frequency. To compute the amplitude and phase of  $S$ -matrix,  $|S[jT, n/NT]|$ , and  $\tan^{-1}(\text{imag}(S[jT, n/NT])/\text{real}(S[jT, n/NT]))$ , respectively, are utilized [28], [29].

### III. EXPERIMENTAL HARDWARE AND DATA ACQUISITION

The set-up for performing the PQ assessment is presented in Fig. 2. The emulated weak grid consists of a one-phase voltage source of 220 V in series with an inductor of 30 mH

TABLE I  
CHARACTERISTIC AND RATINGS OF SOLAR CELL MODULE

Parameter	Rated value
Rated power ( $W_p$ )	230 W ( $\pm 3\%$ )
Max. power voltage ( $V_{mp}$ )	29.3 V
Max. power current ( $I_{mp}$ )	7.84 A
Open circuit voltage ( $V_{oc}$ )	37.1 V
Short circuit current ( $I_{sc}$ )	8.42 A
The temperature coefficient of power	$-0.405 \pm 0.05\%/^{\circ}\text{C}$
The temperature coefficient of voltage	$-0.312 \pm 0.015\%/^{\circ}\text{C}$
The temperature coefficient of current	$+0.075 \pm 0.015\%/^{\circ}\text{C}$

TABLE II  
DAS AND DATA ANALYSIS COMPONENTS

S.No.	DAS component
1	Power quality analyser (WT3000)
2	Voltage transformer
3	Current transformer
4	Laptop Computer 64-bit operating system, 4 GB RAM, Intel(I) Core(TM)i5-3230M CPU@2.60 GHz processor
5	WT viewer software
6	Connecting probes

with short-circuit rating of 5 kVA. It is integrated with an SPV plant of capacity 230 W. The SPV system has the solar cell module, joint box, charge controller, battery, and grid connected inverter. The solar cell module consists of the solar cells of polycrystalline silicon. The characteristics and rated parameters of the solar cell module are provided in Table I. The outdoor SPV panel supplies power to the storage battery of capacity 55 AH, 24 V through the joint box and a battery charge controller. The joint box consists of a fuse and diode for protection of the solar generator. The battery charge controller is the dc-dc converter. Hence, voltage of the input power to this converter is the same as the voltage of the solar module output. Solar PV module operates at maximum power voltage ( $V_{mp}$ ) equal to 29.3 V. Output voltage of the dc-dc converter is 24 V and constant, which is same as the battery voltage. Solar PV module output voltage may change depending on the level of solar insolation. Hence, dc-dc converter eliminates variations in the solar output voltage and gives a constant output voltage. The charge controller controls the charging and discharging of the battery within limits, thereby maximizing the battery life time. Battery is used to compensate variations in the SPV energy production. A dc-ac converter is employed to convert the dc energy produced by the SPV system to ac energy and connects the same to the utility grid at PCC. The output voltage of the dc-ac converter is 230 V, one-phase ac. Pulsewidth modulation controllers are used for the control of the dc-dc converter and dc-ac converter in the hardware set-up [30]–[32].

Fig. 3 presented the DAS installed at PCC for assessing the PQ. Power flows from the SPV module to the utility grid through the path as, PV module  $\rightarrow$  dc-dc converter  $\rightarrow$  dc-ac converter  $\rightarrow$  transformer  $\rightarrow$  current transformer (CT)  $\rightarrow$  PCC  $\rightarrow$  utility grid. An arrow in Fig. 3 indicates this direction of power flow. Components of the DAS are detailed in Table II. The current supplied by the SPV system is recorded with the help of the CT, and the voltage on the PCC is recorded using the potential transformer (PT). PQ analyzer is used to record these voltage

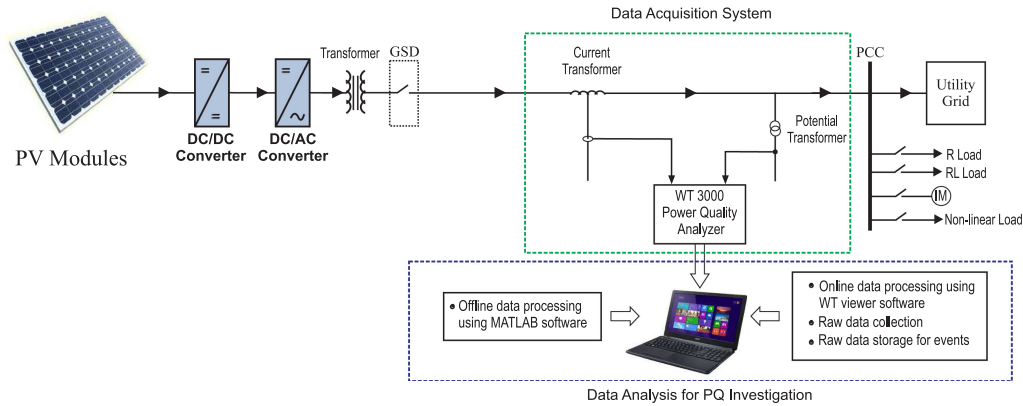


Fig. 3. Measurement system of PQ.

TABLE III  
STATUS OF THE DEMANDS AT PCC

S.No.	Type of load	Rated value
1	Resistive	1-phase, 400 W
2	RL Load	1-phase series combination of 400 W resistive load and 0.90 H, 3.6 $\Omega$ , 660 turns inductive load.
3	Induction motor (IM) load	1-phase, capacitor run, 320 W, 50 Hz, 220 V, 1500 rpm.
4	Non-linear (NL) load	SCR based 1-phase rectifier supplying to resistive load of capacity 200 W.

and current signals. Hence, CT, PT, and PQ analyzer are the main components of the DAS. These recorded data are analyzed using the proposed algorithm with the help of laptop in both the online and offline mode. The data acquisition is performed under the events of interfacing and outage in the accessibility of a variety of loads at PCC. The case of partial shading of the SPV module is also considered. Nature of the demands situated at the PCC include resistive, resistive inductive (RL), induction motor (IM), and nonlinear (NL) as detailed in Table III. Grid synchronization device (GSD) is utilized to connect the PV system at PCC. By closing and opening of the GSD, interfacing and outage operations are performed in this study.

Various case studies associated with the outages are represented as C1-0–C1-4 whereas studies associated with the synchronization is designated as C2-0–C2-4 and detailed in Table IV.

#### IV. CASE STUDIES OF PQ ASSESSMENT

The experimental set-up detailed in Section III, is utilized to create the outage and interfacing of SPV plant with the grid in the accessibility of various types of loads at PCC. The outage and interfacing are carried out with the help of GSD. The voltage signal captured at PCC is processed by utilizing multiresolution investigation based on  $S$ -transform. This analysis is compared with that of standard PQ disturbances reported in [22] and [23]. PV array output voltage and dc–dc converter output voltage obtained from the recorded time series data are described in Fig. 4(a) and (b), respectively. These values are constant and

TABLE IV  
OPERATING SCENARIOS

Case No.	Class symbol	Event description
1	C1-0	PV outage from grid in the absence of load at PCC.
2	C1-1	PV outage from grid in the availability of resistive load at PCC.
3	C1-2	PV outage from grid in the availability of RL load at PCC.
4	C1-3	PV outage from grid in the availability of induction motor as a load at PCC.
5	C1-4	PV outage from grid in the availability of non-linear load at PCC.
6	C2-0	PV interfacing with grid in the absence of demand at PCC
7	C2-1	PV interfacing with grid in the availability of resistive load at PCC.
8	C2-2	PV interfacing to the grid in the availability of RL demand at PCC.
9	C2-3	PV interfacing to the grid in the availability of induction motor as load at PCC
10	C2-4	PV interfacing to the grid in the availability of non-linear load at PCC.

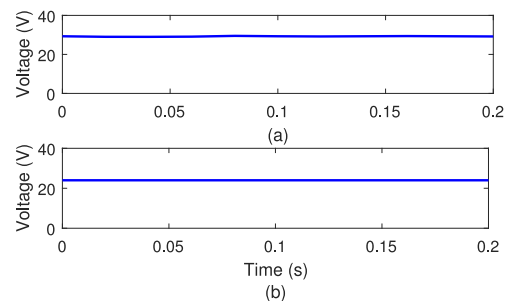


Fig. 4. (a) PV array output voltage. (b) DC–DC converter output voltage.

equal to rated values of 29.3 and 24 V in respective order. However, the change in solar insolation may slightly deviate the PV array output voltage. DC–DC converter output voltage remains constant because variations in the voltage are absorbed by the battery and charge controller. Various case studies are illustrated in the following sections.

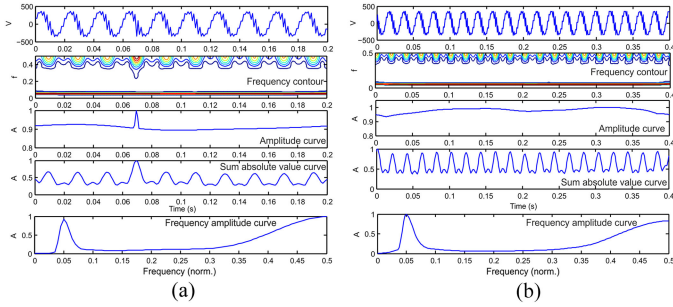


Fig. 5. (a) Voltage waveforms and respective  $S$ -transform supported plots with outage of SPV plant and no load at PCC. (b) Voltage waveforms and respective  $S$ -transform supported plots with the interfacing of SPV plant to grid and no load at PCC.

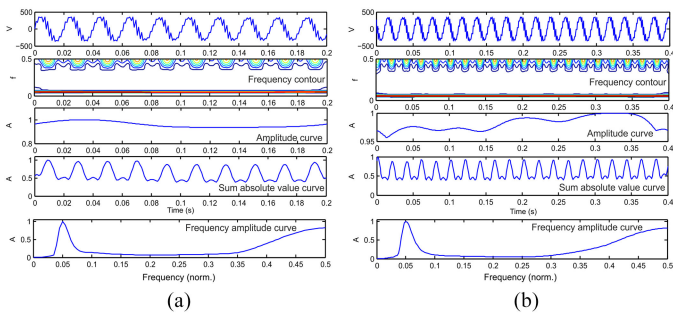


Fig. 6. (a) Voltage waveforms and respective  $S$ -transform supported plots with outage of SPV plant and resistive load at PCC. (b) Voltage waveforms and respective  $S$ -transform supported plots with the synchronization of SPV plant to grid and resistive load at PCC.

### A. No Demand Available at PCC

In the fourth cycle, the outage of SPV plant from the grid is performed by opening the GSD. Fig. 5(a) presents the related  $S$ -transform depended plots of voltage signal at PCC. Its presence is shown by the peaks available in the AM and SAV plots. A contour with a small peak in the FC, also indicates the same. Low amplitude voltage sag is found in the AM plot. Increase in the amplitude of the FM curve after 0.30 of normalized frequency shows the occurrence of high-frequency harmonics in the voltage single.

The SPV plant is synchronized with grid in the first cycle. Fig. 5(b) presents the  $S$ -transform depended curves of voltage waveforms. Voltage swell is identified by rise in magnitude of the AM plot whereas variation in the amplitude also illustrates the voltage fluctuations. Harmonics' presence is shown by continuous spikes, existing on the surface of the SAV plot. Furthermore, harmonics are also indicated by the upper portion of the FC. Increase in the magnitude of FM plot beyond the normalized frequency of 0.35 identifies the harmonics of higher order.

### B. Resistive Demand at PCC

In the fourth cycle, outage of the SPV system is performed and the  $S$ -transform based curves of voltage signals associated with this outage event are presented in Fig. 6(a). Decreased magnitude of AM plot detects sag in the voltage. Rise in the

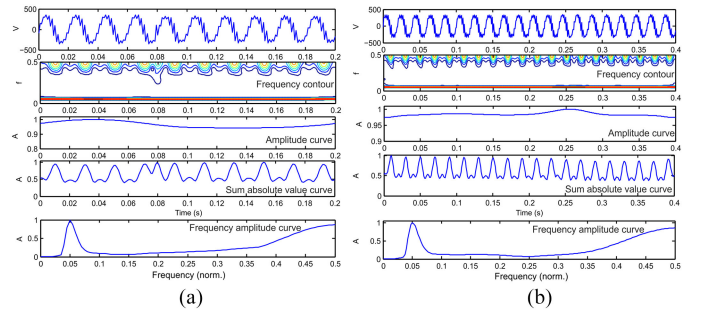


Fig. 7. (a) Voltage waveform and respective  $S$ -transform supported plots with outage of SPV plant and RL load at PCC. (b) Voltage waveform and respective  $S$ -transform supported plots with the interfacing of SPV plant to grid and RL load at PCC.

magnitude of FM plot above normalized frequency of 0.35 indicates availability of the harmonics of higher order.

In the first cycle, the SPV system is interfaced to the grid in the accessibility of resistive load at PCC. Fig. 6(b) illustrated the  $S$ -transform depended plots of voltage signal. Increased magnitude of AM plot detects swell in the voltage. Presence of the voltage fluctuations and flickers is indicated by the sustained deviations in the AM plot. Availability of the harmonics is indicated by the continuous spikes present on surface of the SAV plot. The rise in the amount of FM plot beyond 0.3 of normalized frequency identified as the accessibility of higher order harmonics.

### C. RL Demand at PCC

At the fourth cycle, outage of the SPV system from the network of utility is performed in the accessibility of RL load at PCC. The associated  $S$ -transform depended curves of voltage waveforms are illustrated in Fig. 7(a). A salient contour in the FC at 0.08 s detects the availability of OT. The decreased magnitude of AM plot presents the accessibility of voltage sag. Variation in the nature of ripples on plane of the SAV plot at the instant of outage of the SPV plant indicates the additional harmonics injected. The increasing trend in the FM curve beyond the normalized frequency of 0.15 indicates that wide range of harmonics are present after the outage.

At the 12th cycle, the SPV system with the RL load at PCC is interfaced with the grid. The corresponding  $S$ -transform depended curves of voltage waveforms are shown in Fig. 7(b). Increased magnitude of AM plot illustrates the occurrence of swell in the voltage waveform, followed by the synchronization. The finite value of the FM curve beyond the normalized frequency of 0.35 indicates the accessibility of harmonics of the higher order whereas finite amplitude between normalized frequencies among 0.15–0.3 present the availability of lower order harmonic components.

### D. IM Connected at PCC

The outage of the SPV system from the utility in the accessibility of IM load is computed in the fourth cycle. Fig. 8(a) details the associated  $S$ -transform depended plots of voltage waveforms. The availability of IT is recognized by peaks of high

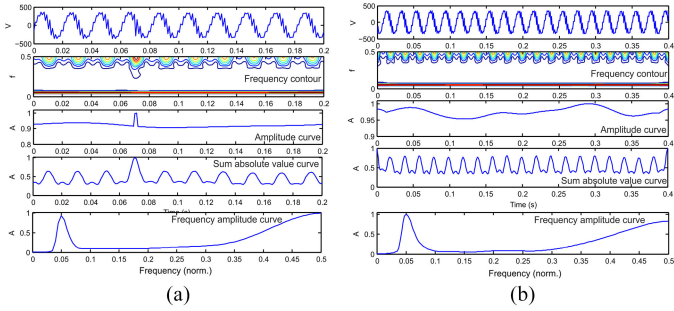


Fig. 8. (a) Voltage waveforms and respective  $S$ -transform supported plots with outage of SPV plant and IM demand at PCC. (b) Voltage waveforms and respective  $S$ -transform supported plots with the synchronization of SPV plant to grid and IM demand at PCC.

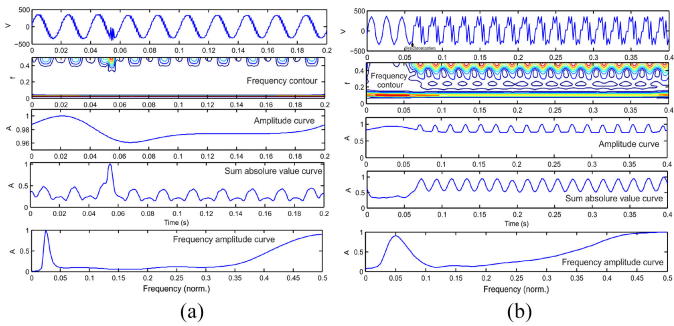


Fig. 9. (a) Voltage waveforms and respective  $S$ -transform supported plots with outage of SPV plant and NL load at PCC. (b) Voltage waveforms and respective  $S$ -transform supported plots during event of synchronization of solar PV plant to grid and NL load at PCC.

magnitude in the AM and SAV curves. The projected contour at 0.07 s in FC detects the availability of OT. AM curve presented the voltage sag of low magnitude. Availability of the harmonics of higher order is detected by the finite values in the FM curve above 0.35 of normalized frequency.

In the second cycle, the  $S$ -transform-based curves of voltage waveform with grid interfacing of the SPV system in the accessibility of IM load is computed and detailed in Fig. 8(b). It is deduced from the amplitude curve that the voltage swell is present followed by the synchronization. It also created the voltage fluctuations and flickers. Finite values of FM curve beyond the normalized frequency of 0.18 illustrated the occurrence of a wide range of harmonics with the higher order harmonics beyond the normalized frequency of 0.35.

### E. NL Demand at PCC

An SCR-based one-phase converter feeding power to the resistive demand of rating 200 W is linked at PCC to investigate the PQ issues in the events of grid synchronization and outage of the SPV system. The outage of the SPV system from the utility in the existence of NL demand is initiated in the third cycle. The respective  $S$ -transform depended curves of voltage waveforms are presented in Fig. 9(a). A salient contour in the FC presents the availability of OT. Decreased magnitude of the AM plot indicates the presence of voltage sag for a duration of

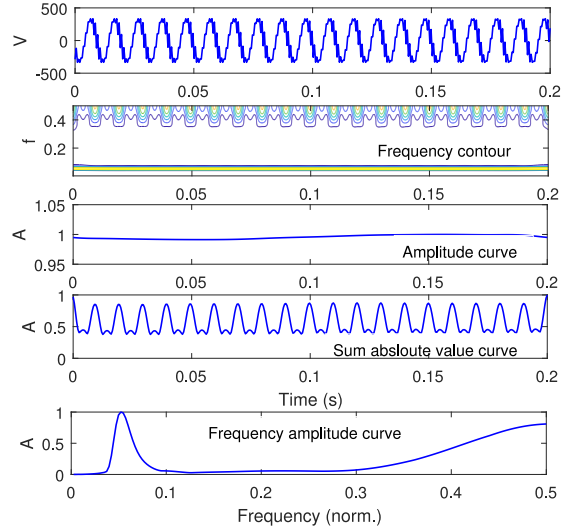


Fig. 10. Voltage waveforms and respective  $S$ -transform supported plots with partial shading and resistive load at PCC.

0.02 s. A large peak in the SAV curve indicates the presence of IT. A wide range of harmonics is detected by increasing order of FM curve over entire range of the normalized frequency.

The SPV system with NL demand (described earlier) at PCC is synchronized to the grid in the third cycle (0.06 s). The related  $S$ -transform depended curves of voltage waveforms are presented in Fig. 9(b). The continuous train of circular contours in the FC presents the availability of notches. Sustained ripples in the upper portion of the FC indicate the harmonics. Ripples on the SAV curve after the synchronization event illustrate the occurrence of harmonics. Rise in the amplitude of harmonics with the order is illustrated by the continuous increase in the FM curve with normalized frequency.

### F. Effect of Partial Shading

For investigating the consequence of partial shading on the PQ of supplied energy by the solar PV plant, 33% of the SPV module area is covered. A resistive load of 400 W (one-phase) is connected at the PCC. The voltage signal and respective  $S$ -transform-based curves of voltage waveforms for the event of partial shading are presented in Fig. 10. It is observed that due to the event of partial shading, the PQ problems linked with the change in voltage amplitude such as sag, swell, and MI are not observed. However, harmonics are detected by increasing order of FM curve throughout the range of normalized frequency.  $THD_v$  and  $THD_i$ , respectively, are observed as 0.531% and 2.421%. Hence, partial shading of the PV modules introduces the PQ issues related to the harmonics. The sudden change in the shading is not investigated due to the experimental limitation.

### G. Harmonic Analysis

The single-sided amplitude spectrum of voltage and current signals computed using the Fast FT during the operation of grid synchronization of the solar PV plant in the existence of resistive load as illustrated in Fig. 11(a) and (b), respectively.



TABLE V  
THDs OF CURRENT

Nature of load	$THD_i$ obtained using PQ Analyser		$THD_i$ (FFT Results)		Error (%)	
	Outage (C1)	Synchronization (C2)	Outage (C1)	Synchronization (C2)	Outage (C1)	Synchronization (C2)
No load (0)	6.224	4.115	6.085	4.045	2.233	1.701
Resistive load (1)	5.995	2.985	5.980	2.957	0.250	0.938
RL load (2)	5.002	3.786	5.051	3.890	-0.979	-2.747
Induction motor load (3)	8.601	4.325	8.418	4.271	2.127	1.248
Non-linear load (4)	18.3179	12.962	18.409	12.804	-0.497	1.219

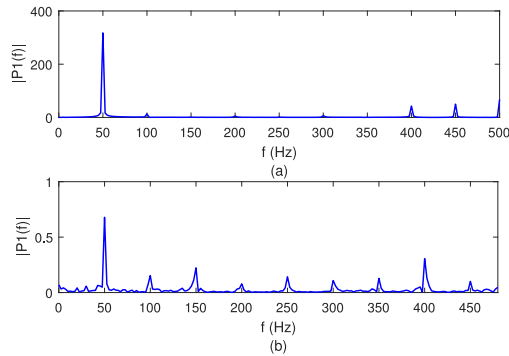


Fig. 11. Single-sided amplitude spectrum during event of grid synchronization of solar PV plant in the presence of resistive load. (a) Voltage signal. (b) Current signal.

It is observed that higher order harmonics are presented in the voltage and current signals. However, the magnitude of higher order harmonics is more dominant in current signals compared to the voltage signals. Due to the space limitation, the spectrum analysis is not discussed for all events. However, the comparative study of THD in voltage and current is included in this section.

$THD_i$  have been obtained using WT 3000 PQ analyzer, used in the experimental set-up, for all the investigated events and provided in Table V. Furthermore, the results obtained by the FFT analysis are also included in this table. An error is computed between the results obtained by the PQ analyzer and computed using FFT to show the effectiveness of the proposed algorithm. Error is computed using the following relation:

$$E = \frac{TE - TS}{TE} \times 100 \quad (9)$$

where  $E$  percentage error in computation of THD in current, TE:  $THD_i$  recorded using WT 3000 PQ analyzer, TS:  $THD_i$  computed using FFT analysis. It is observed from Table V that percentage error in the THD values recorded using the PQ analyzer and computed using FFT is less than 3%. Hence, proposed algorithm effectively identifies the THD during the investigated events.

Magnitude of the disturbances observed during the different events/scenario discussed in above-mentioned sections is small due to the low solar energy penetration level. Due to the limitation of available hardware this penetration level can not be increased. Magnitude of the PQ disturbances will increase with increase in level of solar energy penetration, which also be effectively recognized by the proposed algorithm. This algorithm effectively recognizes any type of PQ disturbance available in the signal. However, magnitude of PQ disturbance associated with the signal will depend on the source and nature of grid, level of solar energy, converters, loads etc.

TABLE VI  
THDs OF CURRENT AND VOLTAGE

Nature of load	$THD_v$		$THD_i$	
	Outage (C1)	Synchronization (C2)	Outage (C1)	Synchronization (C2)
No load (0)	2.571	1.182	6.085	4.045
Resistive load (1)	2.805	1.194	5.980	2.957
RL load (2)	2.672	0.908	5.051	3.890
Induction motor load (3)	3.208	1.816	8.418	4.271
Non-linear load (4)	11.362	9.071	18.409	12.804

TABLE VII  
MAXIMUM FREQUENCY VARIATION AND PQI

Nature of load	Maximum Frequency Deviation		Power Quality Index	
	Outage (C1)	Synchronization (C2)	Outage (C1)	Synchronization (C2)
No load (0)	0.037	0.287	4.3186	8.0417
Resistive load (1)	0.027	0.219	4.8670	9.9602
RL load (2)	0.042	0.312	5.2646	11.3496
Induction motor load (3)	0.048	0.369	5.6452	11.7474
Non-linear load (4)	0.183	0.816	19.5354	28.0251

## V. CASE STUDIES: COMPARISON

All the investigated events have been compared to rate in terms of PQ using the values of THD, maximum deviations in frequency and values of PQI. THD of voltage ( $THD_v$ ) and current ( $THD_i$ ) calculated using FFT and presented in Table VI. It can be seen from the values that  $THD_v$  and  $THD_i$  are more in case of outage event compared to the synchronization event. Highest values of  $THD_v$  and  $THD_i$  are found with NL load at PCC compared to the various kinds of demands in both the events of synchronization and outage. The next level of THDs is found with IM load at PCC. It is seen that the values of  $THD_v$  are less in the presence of RL load compared to the resistive load at PCC.

Table VII presents the maximum frequency deviations and PQI for the outage and synchronization events with different types of loads at PCC. It can be observed that the frequency deviations are more in case of synchronization compared to those associated with the outage. Maximum frequency deviation in case of outage event is found with the NL load at PCC followed by the IM, RL load, no-load, and resistive load. The same trend of frequency deviations can also be observed with the synchronization. Values of PQI are more in case of synchronization compared to those associated with the outage. Value of PQI for outage cases is maximum with the NL load followed by IM load, RL load, resistive load, and no load. The same trend is observed with the synchronization event.

## VI. CONCLUSION

This article provided the PQ evaluation of grid interfaced with an SPV system under various operating conditions using  $S$ -transform. A grid integrated SPV is emulated in the laboratory to assess PQ problems linked to the synchronization and outage of the SPV system with different types of load at PCC. The

